# Quantum Disorder Induced by Nuclear Tunneling in Lattice

Yu-Cheng Zhu,[1] Jia-Xi Zeng,[1,*] Qi-Jun Ye,[1,2] and Xin-Zheng Li[1,2,3,†]

[1]State Key Laboratory for Artificial Microstructure and Mesoscopic Physics, Frontier Science Center for Nano-optoelectronics and School of Physics, Peking University, Beijing 100871, People's Republic of China

[2]Interdisciplinary Institute of Light-Element Quantum Materials, Research Center for Light-Element Advanced Materials, and Collaborative Innovation Center of Quantum Materials, Peking University, Beijing 100871, People's Republic of China

[3]Peking University Yangtze Delta Institute of Optoelectronics, Nantong, Jiangsu 226010, People's Republic of China

(Received 16 January 2025; accepted 28 May 2025; published 20 June 2025)

Lattice degrees of freedom (d.o.f.) may induce quantum disorder (QD) when nuclear tunneling outvies long-range order, but conventional phonon theory is incapable of describing such QD phases. Here we develop a method based on path-integral molecular dynamics to solve this problem. Its accuracy is verified in a double-well chain model and it is applied to a real material from first principles. A quantum order-disorder-order phase transition sequence is demonstrated when varying the strength of quantum fluctuations using the lattice constants as the tuning factor. Combining the excitation spectra and Rényi entanglement entropy, we pinpoint the QD region. This picture may be general in lattice systems having soft phonon modes, not limited to quantum paraelectricity, in which novel entangled lattice motion and its coupling with other d.o.f. can be expected.

DOI: 10.1103/9gkl-w2lm

Quantum disorder (QD) is at the forefront of questing many-body physics and exploring novel quantum materials. Starting from the early days of quantum mechanics, QD has been proposed in spin models whose long-range order of ground state is suppressed by quantum fluctuations [1–4]. Quantum spin liquid, a prototypical example, has been a focus of research interest in recent years due to its potential in exhibiting exotic properties such as topological order and fractionalized excitation [5–7]. Apart from manifesting an intrinsic spin liquid in magnetic systems, budding attention is also paid to the lattice degrees of freedom (d.o.f.) [8,9]. Existing experiments indicate that quantum paraelectricity (QPE) are QD phases [10,11]. However, such cognition stays at a hypothetical level due to lack of description of quantum entangled lattice dynamics and clarification on QD region.

One main difficulty for the absence of these studies is that conventionally the lattice d.o.f. are treated by phonon, which is perturbative and may fail in systems with soft phonon modes at low temperatures. The soft phonon mode indicates multiple degenerate wells on local Born-Oppenheimer potential energy surface (PES) and a structural instability [12] as sketched in Fig. 1. When the barrier between the wells is not uncrossable, one can expect coupling between the wells which gives rise to uncertainty and quantum fluctuations (QF) [13]. This coupling is characterized by nuclear tunneling [14]. Phonon is inefficient to expand the coupling and describe the quantum entanglement in this scenario. In fact, QD on the soft mode is speculated by a phenomenological analogy to models like quantum Ising chain [2,15–17]. Missing of atomic details leads to controversies, e.g., some explanations of the soft modes are based on rattling whilst others are based on anharmonic correction [18–20]. Evidences other than dielectric constants are required both experimentally and theoretically to clarify such controversies, especially for soft mode without an electrical dipole. In QPEs like $SrTiO_3$, $KTaO_3$, and $BaFe_{12}O_{19}$, it is already known that rich physics may arise due to competition between the nuclear QF and intersite interactions, which is sensitive to external factors, such as pressure, strain, and doping [21–26]. To clarify the rich physics behind such substance, a theoretical method beyond the conventional phonon theory for lattice dynamics is clearly needed.

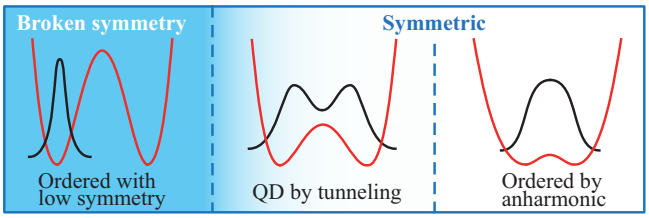


FIG. 1. Schematic diagram of the order-disorder-order phase transition sequence. The red and black curves sketch PES of soft modes and nuclear density distribution, respectively. When the barrier is high (low), the system has low (high) symmetry. In between, there is a QD region where the equilibrium structure has high symmetry but the nuclear density distribution is broad.

*Contact author: hank@pku.edu.cn
†Contact author: xzli@pku.edu.cn

 © 2025 American Physical Society

Here, we develop a method for lattice dynamics to incorporate quantum entanglement from nuclear QF. This method is based on path-integral molecular dynamics (PIMD), which is rigorous in describing nuclear quantum effects including quantum entanglement and quantum tunneling and has been mature for distinguishable continuous-space systems [27–29]. We obtain the excitation spectra from the free energy surface (FES) which is constructed by centroid potential of mean force of PIMD and includes the effects of quantum entanglement and quantum tunneling. Its accuracy in describing QD phases is demonstrated in a double-well chain model by comparing with the exact solution. We then apply it to a real material with the Born-Oppenheimer PES constructed by combining *ab initio* calculation and machine learning techniques. We find an order-disorder-order phase transition sequence with decreasing barrier for quantum tunneling. From an ordered phase with low symmetry, the onset of QF drives the system into a QD phase (Fig. 1). Further reducing the barrier, the QF from nuclear tunneling vanishes and the system goes into an ordered phase with high symmetry. The first transition distinguishes between equilibrium structure with broken and high symmetry, and the second divides tunneling- and anharmonic-dominated phases. The two quantum phase transitions can be characterized by divergences of Rényi entanglement entropy.

We start from a double-well chain model. This is a minimal model for order-disorder phase transitions, which has been used to study ferroelectrics, with one degree of freedom lying on a local double-well potential on each site and springlike interaction between sites [30] [Fig. 2(a)]. In general, with a quartic double well and quadratic spring, the Hamiltonian reads,

$$H = \sum_n \left[\frac{P_n^2}{2m} + A(x_n^2 - R^2)^2 + \frac{1}{2}k(x_n - x_{n+1})^2\right], \quad (1)$$

where $x_n$ is the relative position on site $n$, i.e., $x_n = u_n - nl$ with $l$ being the lattice constant. Each double-well has two local minima at $nl \pm R$. We set $A = 0.00461$ a.u. and $m$ as the mass of a proton. $R$ and $k$ control the shape of barrier and the spring strength respectively. To simplify, we assume a periodic boundary and rewrite the Hamiltonian as

$$H = \sum_n \left[\frac{P_n^2}{2m} + A(x_n^2 - \tilde{R}^2)^2 - kx_n x_{n+1}\right] \quad (2)$$

with a constant neglected and $\tilde{R}^2 = R^2 - k/2A$. The local basis was chosen as the eigenstates $\{|i_n\rangle\}$ of the reshaped double-well $h_n = P_n^2/2m + A(x_n^2 - \tilde{R}^2)^2$. The two lowest levels $i = 0,\ 1$ are the symmetric and antisymmetric superposition states, respectively, whose energy difference $\Delta = E_1 - E_0$ is called the tunneling splitting. Then the above Hamiltonian transforms to

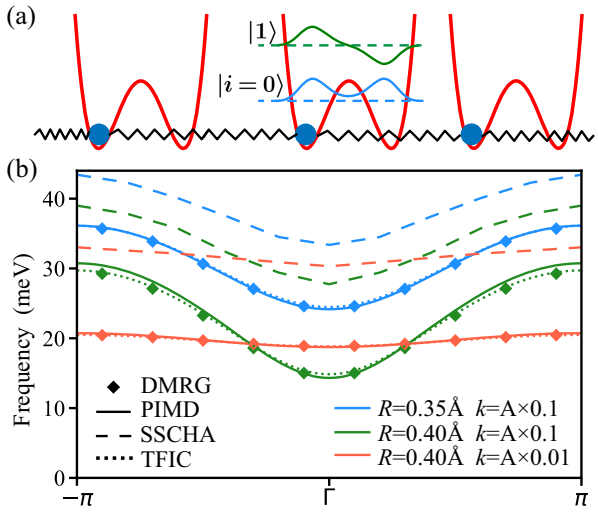


FIG. 2. (a) A schematic diagram of 1-D double-well chain. One degree of freedom (the ball) lies on a double-well potential (red curve) connected to neighboring site by spring interaction (zigzag lines). (b) Excitation spectra of 1-D double-well chain. The DMRG (diamonds), PIMD (solid lines) and TFIC (dotted lines) are in good agreement. SSCHA (dashed lines) overestimates the excitation energies because of its shortcoming in describing tunneling. The blue (red) lines are spectra of chain with low (high) barrier and strong (weak) spring.

$$\hat{H} = \sum_n \hat{h}_n - k\sum_n \hat{X}_n\hat{X}_{n+1} \quad (3)$$

with $\hat{h}_n = \sum E_i|i\rangle\langle i|$ and $\hat{X}_n = \sum_{i,j}|i\rangle\langle i|\hat{x}_n|j\rangle\langle j|$. The first onsite term provides QF by nuclear tunneling, while the second intersite term prefers ordering such as ferroelectricity. If retaining only the two lowest levels in local basis, one arrives at the transverse-field Ising chain (TFIC) $\hat{H} = \tilde{\Delta}\sum\hat{\sigma}_n^z - \tilde{k}\sum\hat{\sigma}_n^x\hat{\sigma}_{n+1}^x$, which gives a QD phase when $\tilde{\Delta} > \tilde{k}$ [4,31].

Eq. (3) can be precisely solved by the density matrix renormalization group (DMRG) method [32–34]. The first excitation band is shown in Fig. 2(b) for different parameters used in Eq. (2). The single-particle excitation bands of TFIC are very close to the DMRG ones, supporting that (1) the "two-levels" approximation is reasonable in describing the QD phase; (2) the QD phase is induced by nuclear tunneling. Then we look at the solid lines from our new method based on PIMD. Its idea is that one can always extract frequency of a regular motion from the FES, with contributions from thermal and quantum fluctuations taken into account. At low temperatures, one just need force constants by the forces of several finite-displaced structures on FES around the equilibrium structure to obtain excitation spectra. Here, we get the force on FES by centroid potential of mean force in a fixed-centroid PIMD where the centroid is fixed at one of the finite-displaced structures, based on an efficient and high-quality sampling. As shown in Fig. 2(b), for a wide range of barrier height $V_{\text{barrier}} = AR^4$ and spring strength $k$

in disordered phase, the PIMD lines are also in good agreement with the DMRG ones. With $V_{\text{barrier}}$ increasing, the energy gap at Γ point tends to close until a quantum order-disorder phase transition. As an example of neglecting tunneling effect, the stochastic self-consistent harmonic approximation (SSCHA) [35] is shown to overestimate the excitation energy, and the departure becomes serious near the critical point. Considering the fact that SSCHA is prevalent in calculating phonon spectra, we note that its inherent Gaussian density distribution of the nuclear wave function which precludes it from accurate description of tunneling [36] means that one should be cautious for its application in such a scenario.

Compared with DMRG and TFIC, one advantage of our PIMD method is that it is applicable to real materials. So we apply it to $SrTiO_3$ from first principles, with the Born-Oppenheimer PES constructed using a combination of density-functional theory (DFT) and machine learning force field (MLFF). The DFT calculations are performed by the Vienna *Ab initio* Simulation Package (VASP) [37] at GGA level using the Perdew-Berke-Ernzerhof (PBE) functional [38] and projector augmented wave (PAW) pseudopotentials [39]. The machine learning techniques are used to save computational cost so that our PIMD based phonon spectra calculation is doable [40–42]. Here we employ the MLFF method built in VASP in view of its reliability for crystals as demonstrated by Verdi el al. [25,43] As a practical test on its accuracy, the harmonic phonon spectra (by Phonopy software [44]) in comparison with the DFT one is shown in Fig. S1 [45]. Then, the PIMD simulations are performed using the I-PI software [46] with self-developed implementations for excitation spectra and Rényi entanglement entropy calculations. We fix the centroid at finite-displaced structures (0.03 Å from equilibrium position) when sampling centroid potential of mean force and define particular normal modes according to the "replica exchange" technique [47] when calculating the Rényi entropy. More computational details are shown in Supplemental Material [45].

$SrTiO_3$ has a cubic perovskite phase ($Pm\bar{3}m$) at room temperature, which transforms to a tetragonal one ($I4/mcm$) below 105 K. This first-order phase transition is driven by the $A_{1g}$ component of an antiferrodistortive (AFD) mode where two adjacent oxygen octahedras in $ab$ plane rotate reversely around $c$ axis [48]. From the harmonic phonon spectra by DFT, the $E_g$ components of AFD mode [as marked by black arrows in Fig. 3(a)] is soft at $T = 0$ K, similar to the ferroelectrical (FE) mode. This soft FE mode is responsible for its QPE [17]. The AFD $E_g$ mode (referred to as AFD mode below) is sensitive to the uniaxial tension of lattice, while the FE mode is coupled with uniform pressure [Figs. 3(b) and 3(c)] [49,50]. Thus, a tiny change in lattice constants would affect the softness of these modes and $SrTiO_3$ is an incipient ferroelectric. The strain sensitivity also means that it is of good

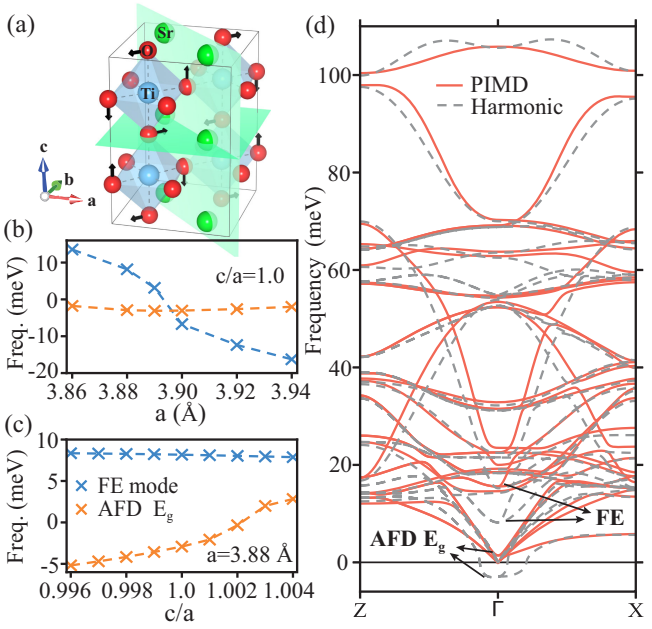


FIG. 3. (a) Structure of a unit cell of tetragonal $SrTiO_3$ ($I4/mcm$). The black arrows sketch the $E_g$ component of AFD mode. (b) and (c) show frequencies of FE and AFD modes at Γ point by harmonic phonon when varying $a$ and $c/a$. The FE and AFD modes are sensitive to $a$ and $c/a$, respectively. (d) The excitation spectra of tetragonal $SrTiO_3$ ($I4/mcm$) with $a, c =$ 3.88 Å by PIMD at 6 K (red lines) and harmonic phonon (gray dashed lines). The AFD mode is lifted from an imaginary frequency to ∼2 meV.

operability to control the softness of these modes and related properties. To study the QPE phenomenon and focus on the soft FE mode, large values of $c/a$ ratio were often used in previous simulations [43,50], which exclude the softness of AFD mode [Fig. 3(c)].

For a clear demonstration of the picture of QD, other than the FE mode, we focus on the AFD mode, which is more representative of general soft modes in lattice without electric dipoles. This is enabled by increasing uniform pressure to exclude the softness of the FE mode, so that only the AFD mode is soft. Here we set the lattice constant $a = 3.88$ Å, which is smaller than the relaxed lattice constant of PBE ($a = 3.93$ Å) by 1.3% and smaller than the experimental lattice constant ($a = 3.896$ Å) by 0.4%. As in Fig. 3(d), with $a = 3.88$ Å and $c/a = 1.0$, the AFD (FE) mode has an imaginary (real) frequency in harmonic phonon spectrum. The spectra of primitive cell are shown by the gray dashed (red solid) lines for the harmonic (PIMD) results. In the PIMD simulation, 128 beads are used for a $3 \times 3 \times 3$ supercell of primitive cell ($I4/mcm$). Except for the AFD and FE modes, other optical phonon modes are just slightly corrected by PIMD. Although without a local degeneracy, the FE mode is still lifted to a higher frequency because of strong scattering with other phonon. This anharmonic effect can be described by

methods with atomic details like SSCHA but is neglected in model studies like TFIC or Vanderbilt model Hamiltonian [17]. However, the SSCHA has been shown to fail for tunneling effect. So, a unified theory from first principles is indispensable to quantify the delicate interplay between tunneling and anharmonic effects. The soft AFD mode is also lifted to a positive frequency with a gap at Γ point of about 2 meV. It is unclear whether this lift comes from tunneling or anharmonic effect, which leads to a controversy. To clarify this, we vary the softness of AFD mode by $c/a$ to control the strength of nuclear QF. Meanwhile, the frequencies of modes other than AFD remain unchanged. So we can separate variables and focus on AFD mode in the following. We perform PIMD simulations using a $3 \times 3 \times 3$ supercell of unit cell to mitigate the finite size effect. The unit cell of tetragonal $SrTiO_3$ contains 20 atoms and has lattice constants of $(\sqrt{2}a, \sqrt{2}a, 2c)$.

By varying the $c/a$ ratio, we found that the gap approaches zero at $c/a = 0.9995(0.9993)$ when 128 (64) beads are used in the PIMD simulations at $T = 6$ K [Fig. 4(a)]. The closure of this gap means a phase transition from an ordered phase with a statistically low symmetry to a QD phase whose equilibrium structure has a high symmetry. This can be confirmed by further calculations

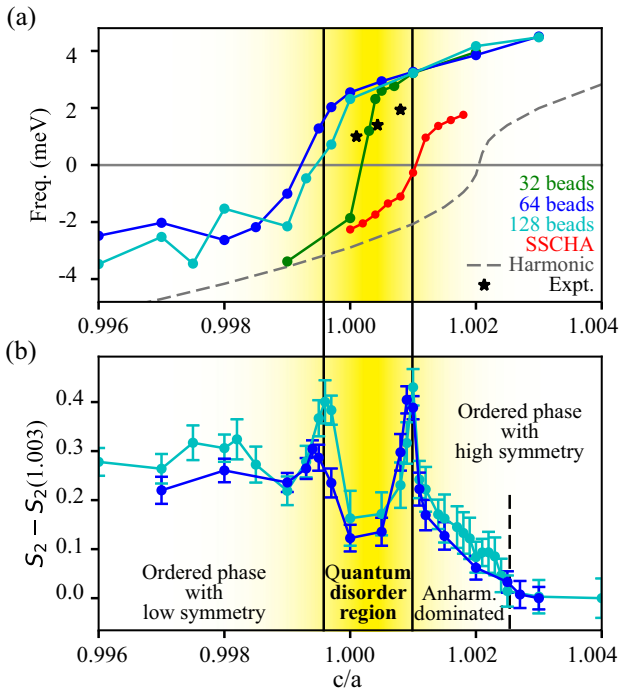


FIG. 4. (a) Gap of AFD mode with varying $c/a$. A structural phase transition is expected when the gap closes. The PIMD approaches convergence with 128 beads and gives distinct critical point compared with SSCHA and harmonic phonon. (b) the Rényi entanglement entropy by PIMD. The two peaks correspond to two quantum phase transitions (black vertical lines), both important in pinpointing the QD phase, which is highlighted by yellow blocks.

of the Rényi entanglement entropy $S_\alpha = (1/1-\alpha)\ln \mathrm{Tr}\rho_A^\alpha$ with $\alpha = 2$ by PIMD. Here, we choose the 12 oxygen atoms in one of the unit cells as the subregion B and the rest of the supercell as subregion A. $\rho_A$ is the reduced density matrix of A. We use the "replica exchange" technique in the path integral [47] of $\mathrm{Tr}\rho_A^2$ and apply a thermodynamic integration (TI) to achieve high-quality sampling. We also employ a path regularization for TI following the work by Miha Srdinsek [51] and the Gauss-Legendre quadrature for integration. As in Fig. 4(b), there is a peak of the Rényi entropy $S_2$ at $c/a = 0.9996$ for 128 beads and $c/a = 0.9994$ for 64 beads. The peak represents a divergence of the entanglement entropy and indicates a quantum phase transition. The critical points by Rényi entropy and by excitation spectra agree well with each other, pinpointing a clear phase transition.

Besides this, after the asymmetric to symmetric phase transition, we note that there is a second peak at $c/a = 1.001$. This peak marks a quantum phase transition in the high-symmetry region, which has not been proposed as we know in literature. Intuitively, when the barrier completely disappears at $c/a = 1.002$ (given by the harmonic phonon), the system must have left the disordered region because the local degeneracy and QF by tunneling have vanished. Therefore, there should be a transition from QD back to ordered phase due to vanishing of local degeneracy. However, strangely, this transition happens before the barrier disappears. Considering the fact that anharmonicity can lift the frequencies of soft phonon compared with the harmonic results, we also calculate the gap using SSCHA with a $3 \times 3 \times 3$ supercell of primitive cell. The results are shown by the red line in Fig. 4(a). The gap closes around $c/a = 1.001$, which is in excellent consistence with our second peak of $S_2$. Therefore, it is the anharmonic effects which bring the transition from $c/a = 1.002$ (harmonic phonon) to 1.001 (SSCHA and our second peak), which accelerates the vanishing of QF by tunneling. As boundary of tunneling and anharmonic effect, we note that the second transition is important in determining the existence of QD region. Our methods on excitation spectra and Rényi entanglement entropy are able to solve the earlier controversies on QD and anharmonicity, and they are predictive for real materials.

We now suggest some criteria to quickly filter out probable soft modes possessing QD behavior. The first one is a temperate barrier which is necessary for strong QF. In some cases, the barrier size and tunneling strength is adjustable by pressure, strain, isotope or doping. This may be responsible for some intricate phenomenon in high-pressure or doped systems, such as Ice VII-VIII-X phase transition and superconducting dome in doped $SrTiO_3$ [52–54]. The second one is a weak intersite interaction. This may be important for systems composed by heavy atoms such as many perovskites and the "electron-crystal

phonon-glass" materials [55]. There are also hints from experiments, such as a wide nuclear density distribution and optical mode with ultralow frequency in scattering spectra [56,57]. The former has been considered an indication of nuclear tunneling. The frequencies, around 1 meV, conform to the energy scale of nuclear tunneling. An example is the 0.5 meV inelastic peak in neutron scattering spectra of $BaTiS_3$ which is proposed to be related to tunneling and responsible for the anomalous glasslike thermal conductivity [58]. In our case, the frequency of AFD mode is around 2 meV and it is close to the value from Raman and neutron spectra [59,60] [black stars in Fig. 4(a)]. Besides these, a feature of special excitation like in quantum spin liquids is also desirable [61]. Ideally, $SrTiO_3$ could be approximated to a 3-D quantum Potts or Ising model. Although a complete description of the latent quasiparticle is still hard because both theoretical and experimental attempts on 3D materials are not yet sprouted, we take a step forward to unravel the quantum many-body physics. Our method on excitation spectra may give some clues. Beyond the adiabatic picture, we also expect that nontrivial coupling with electron and acoustic phonon which may be related to unconventional superconductivity and glasslike thermal conductivity, and we hope the progresses made here can stimulate such investigations.

*Acknowledgments*—We are supported by the National Science Foundation of China under Grants No. 12234001, No. 12404257, No. 12474215, No. 12204015, and No. 62321004, and the National Basic Research Program of China under Grants No. 2021YFA1400500, and No. 2022YFA1403500. The computational resources are provided by the supercomputer center at Peking University, China.

*Data availability*—The data supporting this study's findings are available within the article.

[1] R. Kubo, The spin-wave theory as a variational method and its application to antiferromagnetism, Rev. Mod. Phys. **25**, 344 (1953).
[2] P. Pfeuty, The one-dimensional ising model with a transverse field, Ann. Phys. (N.Y.) **57**, 79 (1970).
[3] L. Amico, R. Fazio, A. Osterloh, and V. Vedral, Entanglement in many-body systems, Rev. Mod. Phys. **80**, 517 (2008).
[4] S. Sachdev, *Quantum Phase Transitions*, 2nd ed. (Cambridge University Press, Cambridge, England, 2011).
[5] L. Savary and L. Balents, Quantum spin liquids: A review, Rep. Prog. Phys. **80**, 016502 (2016).
[6] Y. Zhou, K. Kanoda, and T.-K. Ng, Quantum spin liquid states, Rev. Mod. Phys. **89**, 025003 (2017).
[7] C. Broholm, R. J. Cava, S. A. Kivelson, D. G. Nocera, M. R. Norman, and T. Senthil, Quantum spin liquids, Science **367**, eaay0668 (2020).
[8] S.-P. Shen, J.-C. Wu, J.-D. Song, X.-F. Sun, Y.-F. Yang, Y.-S. Chai, D.-S. Shang, S.-G. Wang, J. F. Scott, and Y. Sun, Quantum electric-dipole liquid on a triangular lattice, Nat. Commun. **7**, 10569 (2016).
[9] S. Wang, L. Zhang, and F. Wang, Possible quantum paraelectric state in Kitaev spin liquid candidate $H_3LiIr_2O_6$, Sci. China Phys. Mech. Astron. **63**, 117411 (2020).
[10] K. A. Müller and H. Burkard, $SrTiO_3$: An intrinsic quantum paraelectric below 4 k, Phys. Rev. B **19**, 3593 (1979).
[11] K. A. Müller, W. Berlinger, and E. Tosatti, Indication for a novel phase in the quantum paraelectric regime of $SrTiO_3$, Z. Phys. B **84**, 277 (1991).
[12] J. F. Scott, Soft-mode spectroscopy: Experimental studies of structural phase transitions, Rev. Mod. Phys. **46**, 83 (1974).
[13] R. Brout, K. Müller, and H. Thomas, Tunnelling and collective excitations in a microscopic model of ferroelectricity, Solid State Commun. **4**, 507 (1966).
[14] R. Blinc, On the isotopic effects in the ferroelectric behaviour of crystals with short hydrogen bonds, J. Phys. Chem. Solids **13**, 204 (1960).
[15] P. de Gennes, Collective motions of hydrogen bonds, Solid State Commun. **1**, 132 (1963).
[16] R. Martoňák and E. Tosatti, Path-integral Monte Carlo study of a model two-dimensional quantum paraelectric, Phys. Rev. B **49**, 12596 (1994).
[17] W. Zhong and D. Vanderbilt, Effect of quantum fluctuations on structural phase transitions in $SrTiO_3$ and $BaTiO_3$, Phys. Rev. B **53**, 5047 (1996).
[18] S. Mukhopadhyay, D. S. Parker, B. C. Sales, A. A. Puretzky, M. A. McGuire, and L. Lindsay, Two-channel model for ultralow thermal conductivity of crystalline $Tl_3VSe_4$, Science **360**, 1455 (2018).
[19] T. Tadano and S. Tsuneyuki, Quartic anharmonicity of rattlers and its effect on lattice thermal conductivity of clathrates from first principles, Phys. Rev. Lett. **120**, 105901 (2018).
[20] J. Klarbring, O. Hellman, I. A. Abrikosov, and S. I. Simak, Anharmonicity and ultralow thermal conductivity in lead-free halide double perovskites, Phys. Rev. Lett. **125**, 045701 (2020).
[21] A. A. Sirenko, C. Bernhard, A. Golnik, A. M. Clark, J. Hao, W. Si, and X. X. Xi, Soft-mode hardening in $SrTiO_3$ thin films, Nature (London) **404**, 373 (2000).
[22] C. Collignon, X. Lin, C. W. Rischau, B. Fauqué, and K. Behnia, Metallicity and superconductivity in doped strontium titanate, Annu. Rev. Condens. Matter Phys. **10**, 25 (2019).
[23] M. N. Gastiasoro, J. Ruhman, and R. M. Fernandes, Superconductivity in dilute $SrTiO_3$: A review, Ann. Phys. (Amsterdam) **417**, 168107 (2020), eliashberg theory at 60: Strong-coupling superconductivity and beyond.
[24] X. Zhang, Q.-J. Ye, H. Xiang, and X.-Z. Li, Quantum paraelectricity of $BaFe_{12}O_{19}$, Phys. Rev. B **101**, 104102 (2020).
[25] L. Ranalli, C. Verdi, L. Monacelli, G. Kresse, M. Calandra, and C. Franchini, Temperature-dependent anharmonic phonons in quantum paraelectric $KTaO_3$ by first principles and machine-learned force fields, Adv. Quantum Technol. **6**, 2200131 (2023).

[26] Y. Y. Guo, H. M. Liu, D. P. Yu, and J.-M. Liu, Ferroelectricity and superparamagnetism in Sr/Ti nonstoichiometric $SrTiO_3$, Phys. Rev. B **85**, 104108 (2012).
[27] C. Cazorla and J. Boronat, Simulation and understanding of atomic and molecular quantum crystals, Rev. Mod. Phys. **89**, 035003 (2017).
[28] D. Chandler and P. G. Wolynes, Exploiting the isomorphism between quantum theory and classical statistical mechanics of polyatomic fluids, J. Chem. Phys. **74**, 4078 (1981).
[29] D. Marx and M. Parrinello, Ab initio path integral molecular dynamics: Basic ideas, J. Chem. Phys. **104**, 4077 (1996).
[30] E. K. H. Salje, B. Wruck, and H. Thomas, Order-parameter saturation and low-temperature extension of Landau theory, Z. Phys. B **82**, 399 (1991).
[31] G. B. Mbeng, A. Russomanno, and G. E. Santoro, The quantum Ising chain for beginners, SciPost Phys. Lect. Notes, **82**, 18 (2024).10.21468/SciPostPhysLectNotes.82
[32] S. R. White, Density matrix formulation for quantum renormalization groups, Phys. Rev. Lett. **69**, 2863 (1992).
[33] U. Schollwöck, The density-matrix renormalization group, Rev. Mod. Phys. **77**, 259 (2005).
[34] H. Zhai, H. R. Larsson, S. Lee, Z.-H. Cui, T. Zhu, C. Sun, L. Peng, R. Peng, K. Liao, J. Tölle, J. Yang, S. Li, and G. K.-L. Chan, BLOCK2: A comprehensive open source framework to develop and apply state-of-the-art DMRG algorithms in electronic structure and beyond, J. Chem. Phys. **159**, 234801 (2023).
[35] L. Monacelli, R. Bianco, M. Cherubini, M. Calandra, I. Errea, and F. Mauri, The stochastic self-consistent harmonic approximation: calculating vibrational properties of materials with full quantum and anharmonic effects, J. Phys. Condens. Matter **33**, 363001 (2021).
[36] A. Siciliano, L. Monacelli, and F. Mauri, Beyond Gaussian fluctuations of quantum anharmonic nuclei, Phys. Rev. B **110**, 134111 (2024).
[37] G. Kresse and J. Furthmüller, Efficiency of ab-initio total energy calculations for metals and semiconductors using a plane-wave basis set, Comput. Mater. Sci. **6**, 15 (1996).
[38] J. P. Perdew, K. Burke, and M. Ernzerhof, Generalized gradient approximation made simple, Phys. Rev. Lett. **77**, 3865 (1996).
[39] G. Kresse and D. Joubert, From ultrasoft pseudopotentials to the projector augmented-wave method, Phys. Rev. B **59**, 1758 (1999).
[40] Y.-C. Zhu, S. Yang, J.-X. Zeng, W. Fang, L. Jiang, D. H. Zhang, and X.-Z. Li, Torsional tunneling splitting in a water trimer, J. Am. Chem. Soc. **144**, 21356 (2022).
[41] T. D. Loose, P. G. Sahrmann, and G. A. Voth, Centroid molecular dynamics can be greatly accelerated through neural network learned centroid forces derived from path integral molecular dynamics, J. Chem. Theory Comput. **18**, 5856 (2022).
[42] W. Fang, Y.-C. Zhu, Y. Cheng, Y.-P. Hao, and J. O. Richardson, Robust gaussian process regression method for efficient tunneling pathway optimization: Application to surface processes, J. Chem. Theory Comput. **20**, 3766 (2024).
[43] C. Verdi, L. Ranalli, C. Franchini, and G. Kresse, Quantum paraelectricity and structural phase transitions in strontium titanate beyond density functional theory, Phys. Rev. Mater. **7**, L030801 (2023).
[44] A. Togo, L. Chaput, T. Tadano, and I. Tanaka, Implementation strategies in phonopy and phono3py, J. Phys. Condens. Matter **35**, 353001 (2023).
[45] See Supplemental Material at http://link.aps.org/supplemental/10.1103/9gkl-w2lm for more computational details and convergence tests.
[46] V. Kapil *et al.*, I-PI2.0: A universal force engine for advanced molecular simulations, Comput. Phys. Commun. **236**, 214 (2019).
[47] M. B. Hastings, I. González, A. B. Kallin, and R. G. Melko, Measuring Renyi entanglement entropy in quantum Monte Carlo simulations, Phys. Rev. Lett. **104**, 157201 (2010).
[48] P. A. Fleury, J. F. Scott, and J. M. Worlock, Soft phonon modes and the 110 °K phase transition in $SrTiO_3$, Phys. Rev. Lett. **21**, 16 (1968).
[49] W. Zhong, D. Vanderbilt, and K. M. Rabe, Phase transitions in $BaTiO_3$ from first principles, Phys. Rev. Lett. **73**, 1861 (1994).
[50] D. Shin, S. Latini, C. Schäfer, S. A. Sato, U. De Giovannini, H. Hübener, and A. Rubio, Quantum paraelectric phase of $SrTiO_3$ from first principles, Phys. Rev. B **104**, L060103 (2021).
[51] M. Srdinšek, M. Casula, and R. Vuilleumier, Rényi entropy of a quantum anharmonic chain at nonzero temperature, Phys. Rev. B **108**, 245121 (2023).
[52] M. Benoit, D. Marx, and M. Parrinello, Tunnelling and zero-point motion in high-pressure ice, Nature (London) **392**, 258 (1998).
[53] G. F. Reiter, J. Mayers, and P. Platzman, Direct observation of tunneling in KDP using neutron compton scattering, Phys. Rev. Lett. **89**, 135505 (2002).
[54] J. M. Edge, Y. Kedem, U. Aschauer, N. A. Spaldin, and A. V. Balatsky, Quantum critical origin of the superconducting dome in $SrTiO_3$, Phys. Rev. Lett. **115**, 247002 (2015).
[55] T. Takabatake, K. Suekuni, T. Nakayama, and E. Kaneshita, Phonon-glass electron-crystal thermoelectric clathrates: Experiments and theory, Rev. Mod. Phys. **86**, 669 (2014).
[56] R. P. Hermann, V. Keppens, P. Bonville, G. S. Nolas, F. Grandjean, G. J. Long, H. M. Christen, B. C. Chakoumakos, B. C. Sales, and D. Mandrus, Direct experimental evidence for atomic tunneling of europium in crystalline $Eu_8Ga_{16}Ge_{30}$, Phys. Rev. Lett. **97**, 017401 (2006).
[57] Y. Liu, Q. Xi, J. Zhou, T. Nakayama, and B. Li, Phonon-glass dynamics in thermoelectric clathrates, Phys. Rev. B **93**, 214305 (2016).
[58] B. Sun *et al.*, High frequency atomic tunneling yields ultralow and glass-like thermal conductivity in chalcogenide single crystals, Nat. Commun. **11**, 6039 (2020).
[59] G. Shirane and Y. Yamada, Lattice-dynamical study of the 110°k phase transition in $SrTiO_3$, Phys. Rev. **177**, 858 (1969).

[60] L. Cao, E. Sozontov, and J. Zegenhagen, Cubic to tetragonal phase transition of $SrTiO_3$ under epitaxial stress: An x-ray backscattering study, Phys. Status Solidi A **181**, 387 (2000).

[61] T.-H. Han, J. S. Helton, S. Chu, D. G. Nocera, J. A. Rodriguez-Rivera, C. Broholm, and Y. S. Lee, Fractionalized excitations in the spin-liquid state of a kagome-lattice antiferromagnet, Nature (London) **492**, 406 (2012).